288:5°E) during 21–27 September, 1998 were used for the present analysis. A clear negative phase in N_mF_2 and a G condition were observed on September 25. At middle latitudes, negative ionospheric storms, in general, are attributed to the relative changes in the neutral compositions, namely the $[O]/[N_2]$ ratio (Prölss, 1995). Pavlov and his collaborators (e.g. Pavlov, 1994; Pavlov and Buonsanto, 1996, 1997; Pavlov et al., 1999; Pavlov and Foster, 2001) suggested that the vibrationally excited N_2 and O_2 may play a significant role. However, in some case studies (Mikhailov and Schlegel, 1997; Mikhailov and Foster, 1997) the storm effects were successfully explained without including the effects of vibrationally excited N_2 and O_2 in their ionospheric model. In this paper, we seek to ascertain which mechanism plays a more important role for the negative phase. Another interesting feature is a strong post-midnight N_mF_2 decrease, accompanied by an h_mF_2 increase on September 25 compared to the quiet day. The increase in h_mF_2 is likely to be associated with a strong eastward electric field and with enhanced equatorward winds relative to quiet periods, and a large depletion of ionization results from an increased recombination rate (Buonsanto and Foster, 1993). Simulations will be performed to understand in detail the effect of dynamics and recombination processes.

Basically, the simulation of the ionospheric storms using first-principle models is one of the most challenging tasks of ionospheric physics. Contrary to expectation, in case studies the coupled thermosphere–ionosphere models (Anderson et al., 1998) were found to be no more accurate than the uncoupled ionospheric models which adopt the empirical atmospheric models, such as the MSIS (Hedin, 1991) and HWM (Hedin et al., 1996) models. Furthermore, the MSIS model is believed to represent well a statistical description, but does not capture the local structure and the shorter time scales associated with a particular storm. Considerable work has taken into account the MSIS modifications required to give numerical model results with better matches to observations (e.g. Richards and Wilkinson, 1998; Richards et al., 1998; Zhang et al., 1999; Pavlov and Foster, 2001; Lilensten and Blelly, 2002). More recently, the NRLMSISE-00 model (Picone et al., 2002), the latest version of the MSIS model, has been developed. Although the NRLMSISE-00 model has incorporated more data, the model has not achieved much improvement in representing the rapid atmospheric changes during the storm. Besides, neutral winds are also very important for modeling F-layer phenomena. The best empirical model of thermosphere horizontal winds, HWM93 was constructed by Hedin et al. (1996), and is readily accessible. Many studies show that in some cases there is a large disagreement between the model winds and the observed winds or the equivalent winds from the F-layer peak height h_mF_2 (e.g. Titheridge, 1993; Liu et al., 2003). The HWM model requires more improvement. The solar extreme ultraviolet (EUV) flux that is energetic enough to ionize the upper atmosphere, is very important for theoretical modeling. Several solar flux models (e.g., the EUV94 model (Tobiska, 1994) and the EUVAC model (Richards et al., 1994)) are widely used in the aeronomic calculations. However, there are not enough measurements required to confirm which model is better than others (Pavlov and Buonsanto, 1997). Thus suitable input information for theoretical models, such as accurate knowledge of the neutral composition, neutral winds, and solar EUV fluxes, is necessary to reproduce the observations, especially under disturbed conditions (Prölss, 1995).

Attempts have been made to deduce valuable neutral parameters from the ISR data (e.g., Bauer et al., 1970; Oliver, 1979; Mikhailov and Schlegel, 1997; Mikhailov and Foster, 1997; Zhang et al., 2001, 2002). In this paper, we will extract thermospheric information from ISR ion temperature profiles through solving the energy equation (e.g., Bauer et al., 1970; Oliver, 1979) and from electron density profiles using a data assimilation method (Zhang et al., 2001, 2002) for geomagnetically quiet and disturbed days. Using the derived thermospheric information from the Millstone Hill ISR observations as well as a theoretical ionospheric model, this study will explore physical causes of the ionospheric storm effects above middle latitudes during September 1998. Thus we will answer how to adjust these inputs to reproduce storm effects in the ionosphere during the disturbed periods. We will firstly give a brief description of an ionospheric model in Section 2, describe the data and data assimilation method in Section 3, and then present and discuss our results in Section 4. Summary and conclusions are given in the last section.

2. Model description

A one-dimensional theoretical model has been developed for the mid-latitude ionosphere over the altitude range of 100–600 km. It solves the equations of mass continuity and motion for O^+. Ion densities for O_2^+, NO^+, and N_2^+ are calculated under the assumption of photochemical equilibrium. The solar flux EUVAC model (Richards et al., 1994) is used to define our initial EUV flux, and the absorption and ionization cross-sections are taken from Richards et al. (1994). Meanwhile, the scheme for calculating the secondary ionization is taken from Titheridge (1996). The nighttime EUV fluxes are based on the work of Strobel et al. (1974), and the nighttime photoionization cross-sections are obtained from Huba et al. (2000).

We include 21 chemical reactions, for $O^+(^4S)$, $O^+(^2D)$, $O^+(^2P)$, O_2^+, N_2^+, and NO^+, which are listed in Table 1. The scheme of chemical reactions is somewhat similar to the model of Schlesier and Buonsanto (1999) and Pavlov and Foster (2001) in terms of the reaction rates for stable and meta-stable ions. The updated version of our model with new rate coefficients has been described in the later work of Lei et al. (2004). As emphasized by Pavlov et al. (1999, and references therein), the vibrationally excited N_2 and O_2 have significant effects on the O^+ loss rate. The model includes

Table 1
Chemical reactions and rates included in the ionospheric model $T_{eff} = (m_i T_n + m_n T_i)/(m_i + m_n) + 0.329E^2$, where E is the electric field perpendicular to the geomagnetic field in mV/m

Reaction	Rate coefficient ($m^3\ s^{-1}$) or rate (s^{-1})	Reference
$O + (^4S) + N_2(v=0) \rightarrow NO^+ + N$	$k_{10} = 1.533 \times 10^{-18} - 5.92 \times 10^{-19}\ (T_{eff}/300) + 8.60 \times 10^{-20}\ (T_{eff}/300)^2\ (300\ K \leqslant T_{eff} \leqslant 1700\ K)$ $k_{10} = 2.73 \times 10^{-18} - 1.155 \times 10^{-18}\ (T_{eff}/300) + 1.483 \times 10^{-19}(T_{eff}/300)^2\ (1700\ K < T_{eff} < 6000\ K)$	St.-Maurice and Torr (1978)
$O^+(^4S) + N_2\ (v > 0) \rightarrow NO^+ + N$	$k_1 = \sum_{v=1}^{5} N_2(v) k_{1v}/N_2$ $k_{11} = k_{10};\ k_{12} = 38k_{10};\ k_{13} = 85k_{10};\ k_{14} = 220k_{10};\ k_{15} = 270k_{10}$	Pavlov et al. (1999)
$O^+(^4S) + O_2(v) \rightarrow O_2^+ + O$	$k_2 = 1.7 \times 10^{-17}\ (300/T_n)^{0.77} + 8.54 \times 10^{-17} \times \exp(-3467/T_n)$	Hierl et al. (1997)
$O^+(^2D) + N_2 \rightarrow N_2^+ + O$	$k_3 = 1.5 \times 10^{-16}\ (T_{eff}/300)^{0.5}$	Li et al. (1997)
$O^+(^2D) + O_2 \times O_2^+ + O$	$k_4 = 7.0 \times 10^{-16}$	Johnsen and Biondi (1980)
$O^+(^2D) + O \rightarrow O + (^4S) + O$	$k_5 = 1.0 \times 10^{-16}$	Fox and Dalgarno (1985)
$O^+(^2D) + e \rightarrow O + (^4S) + e$	$k_6 = 7.8 \times 10^{-14}\ (300/T_e)^{0.5}$	Torr and Torr (1982)
$O^+(^2P) + N_2 \rightarrow N_2^+ + O$	$k_7 = 2.0 \times 10^{-16}\ (T_{eff}/300)^{0.5}$	Li et al. (1997)
$O^+(^2P) + N_2 \rightarrow N^+ + NO$	$k_8 = 1.0 \times 10^{-17}$	Rees (1989)
$O^+(^2P) + O \rightarrow O^+\ (^4S) + O$	$k_9 = 4.0 \times 10^{-16}$	Chang et al. (1993)
$O^+(^2P) + e \rightarrow O^+\ (^4S) + e$	$k_{10} = 4.0 \times 10^{-14}\ (300/T_e)^{0.5}$	Rees (1989)
$O^+(^2P) + e \rightarrow O^+\ (^2D) + e$	$k_{11} = 1.5 \times 10^{-13}\ (300/T_e)^{0.5}$	Henry et al. (1969)
$O^+(^2P) \rightarrow O^+\ (^4S) + h\nu$	$A_1 = 0.0833\ s^{-1}$	Kaufman and Sugar (1986)
$O^+(^2P) \rightarrow O^+\ (^2D) + h\nu$	$A_2 = 0.277\ s^{-1}$	Kaufman and Sugar (1986)
$O_2^+ + NO \rightarrow NO^+ + O^2$	$k_{12} = 4.4 \times 10^{-16}$	Lindinger et al. (1974)
$O_2^+ + N \rightarrow NO^+ + O$	$k_{13} = 1.2 \times 10^{-16}$	Fehsenfeld (1977)
$O_2^+ + e \rightarrow O + O$	$k_{14} = 2.0 \times 10^{-13}\ (300/T_e)^{0.7}\ (T_e < 1200\ K)$	Walls and Dunn (1974)
	$k_{14} = 1.6 \times 10^{-13}\ (300/T_e)0.55\ (T_e \geqslant 1200\ K)$	Torr et al. (1976)
$N_2^+ + O \rightarrow NO_+ + N$	$k_{15} = 1.4 \times 10^{-16}\ (300/T_i)^{0.44}$	McFarland et al. (1974)
$N_2^+ + O \rightarrow O^+\ (^4S) + N_2$	$k_{16} = 9.8 \times 10^{-18}\ (300/T_i)^{0.23}$	McFarland et al. (1974)
$N_2^+ + O_2 \rightarrow O_2^+ + N_2$	$k_{17} = 5.0 \times 10^{-17}\ (300/T_{eff})$	Lindinger et al. (1974)
$N_2^+ + e \rightarrow N + N$	$k_{18} = 1.75 \times 10^{-13}\ (300/T_e)^{0.3}$	Peterson et al. (1998)
$NO^+ + e \rightarrow N + O$	$k_{19} = 4.2 \times 10^{-13}\ (300/T_e)^{0.85}$	Torr et al. (1976)

the $O^+(^4S)+N_2(v)$ reaction rate measured by Schmeltekopf et al. (1968), and the reaction rate constants for the first five vibrational levels are obtained from Pavlov et al. (1999) (see Table 1). The analytical approach for the solution of the steady state vibrational quanta continuity equation is used to provide the vibrational temperature T_{vib}, which can give similar results for N_mF_2 and h_mF_2 to the full solution of the vibrational quanta continuity equation (Pavlov and Buonsanto, 1996). The rate coefficients of $O^+(^4S) + O_2(v)$ are given by Hierl et al. (1997) to include the effect of $O_2(v)$.

Ion velocity in the vertical direction, V_{iz}, contains the collision drag effect of neutral winds U_n, electric field drifts V_e, and the plasma diffusion V_{diff}. We now discuss how to derive the thermospheric winds in our model. The modified method of Richards (1991) can be used for deriving the equivalent winds from h_mF_2 with the aid of our ionospheric model, which has been introduced by Pavlov and Buonsanto (1997) to avoid repeatedly running the ionospheric model. The equivalent winds (servo winds) include the effects of neutral winds and $\boldsymbol{E} \times \boldsymbol{B}$ drifts. In our ionospheric model the HWM93 model is also an alternative option to specify the neutral winds.

The measured vertical ion drift V_{iz} from ISR provides a more precise option to estimate the thermospheric winds (V_z-based wind), as discussed by Schlesier and Buonsanto (1999). The observed N_e, T_e and T_i are used to calculate the diffusion velocity, V_{diffz} (ISR). The O^+–O collision frequency, ν_{o^+-o}, is a critical parameter for ionospheric modeling. In our model we take the formula suggested by Pesnell et al. (1993).

The ion continuity equation for O^+ can be solved with an implicit numerical method. For the lower boundary at 100 km, an assumption of photochemical equilibrium is adopted. The observed plasma densities at 600 km are taken as the upper boundary values. Default neutral atmospheric parameters are taken from the NRLMSISE-00 model, and NO density is calculated from the O and N_2 densities (Mitra, 1968). The observed plasma temperatures are also input into the ionospheric model.

3. Data and assimilative method

The Millstone Hill incoherent scatter radar experiment was performed from 1034 UT on September 21, 1998, to

0325 UT on September 27, 1998. The profiles of $N_e(h)$, $T_e(h)$, $T_i(h)$, $V_{iz}(h)$, observed with the ISR zenith antenna, are fitted using a 5-degree polynomial in altitude and then interpolated in time. The ion drift vector at 300 km was obtained from the line-of-sight velocities between 250 and 350 km, using the zenith antenna and the steerable antenna measurements with elevation angles no less than 45°. The drift components perpendicular to the magnetic field line represent the $\boldsymbol{E} \times \boldsymbol{B}$ drifts, and the parallel component can be used to estimate meridional winds (V_p-based wind). In addition, the shape of the ISR spectrum depends on ion composition, so the measured ion and electron temperatures rely on the ion composition model (Schlesier and Buonsanto, 1999; Pavlov et al., 1999). During disturbed periods, the standard Millstone Hill composition model may result in large errors in the measured T_e and T_i. The calculated ion compositions in our ionospheric model are used to correct the measured temperature and electron density by multiplication with the factors of Waldteufel (1971).

Input parameters of the ionospheric model (climatological model values), such as solar flux, neutral winds, the neutral composition and temperature, can be set as adjustable variables to bring in the best match with observed electron profiles (Zhang et al., 2001, 2002). Zhang et al. (2001, 2002) have explored the possibility and ambiguity in deriving multiple parameters from electron density profile data and concluded that it is almost impossible to adjust more than two free parameters simultaneously because of the high binary correlation (large variable correlation) in fitting the N_e profile. In this paper, we will use both $T_i(h)$ and $N_e(h)$ profiles in the data assimilation process for obtaining reliable thermospheric information.

First the steady state ion energy equation is solved to extract the thermospheric parameters. This approach has been widely used to derive the neutral temperature and atomic oxygen densities from ISR data (e.g., Bauer et al., 1970; Oliver, 1979). The observed T_i profiles can be fitted using the two free parameters, namely the exospheric temperature T_{ex} and [O] at the reference altitude. At nighttime $T_i = T_e = T_n$, [O] is unavailable and only T_{ex} can be deduced. During disturbed periods, ion-frictional heating (IFH) may be a possible source of systematic errors in determining T_{ex} and [O]. Applying the method of Litvin et al. (2000), in this case the systematic error is less 30 K in T_{ex} and 4% in [O].

Then we can implement two combinations, i.e., EUV-wind and $[N_2]$-wind, to match the measured and calculated N_e profile. Note that the inferred T_{ex} from observed T_i profiles is fed into NRLMSISE-00 model to produce the self-consistent T_n and $[O_2]$. For this data assimilation study, we consider only the daytime electron profiles, so the derived T_{ex} is also used to produce the nighttime neutral temperature and compositions. An optimal EUV multiplicative factor f_E is obtained with the EUV-wind adjustment. $[N_2]$ is obtained with the $[N_2]$-wind adjustment where f_E is used. For the EUV-wind search, we selected the measured data during September 21–23, because the measured data should be more accurate during the quiet days, as mentioned previously. In addition, it should be noted that we have implemented a $[N_2]$-wind adjustment, but found that the adjustment is not effective on September 25 because of the disappearance of the usual F_2-layer. Thus we only adjust $[N_2]$ as single-variable fit on September 25, whilst the winds are calculated from the measured vertical ion drift V_{iz} using the inferred neutral parameters.

4. Results and discussions

4.1. Solar geophysical conditions

The geophysical indices during September 21–27, 1998, are presented in Fig. 1. The solar activity index, F107, varied between 128 and 144, and its 81-day average was about 131 during this period. Given that the 3-h K_p fluctuated between 0 and 4 on September 21–23, 27, we can consider this period as magnetically quiet, and choose September 22 for a reference quiet day. A sudden storm commencement (SSC) occurred at 2345 UT on September 24, accompanied by a severe storm with AE index up to 1800 nT, D_{st} index down to −207 nT, and a maximum value of K_p of 8^+ on September 25. After undergoing the disturbed days of September 24–26, the magnetic activity returned to normal level by September 27.

4.2. Simulations without correcting the MSIS model

Fig. 2 shows the comparison of calculated N_mF_2 and h_mF_2 using the three wind options and standard MSIS model with the measured data. It is surprising that N_mF_2 during the daytime on September 23, decreases 50% with respect to September 22 values, whereas the day-time N_mF_2 on September 24, increases again, and is larger than that of September 23. This event may result from the changes in the

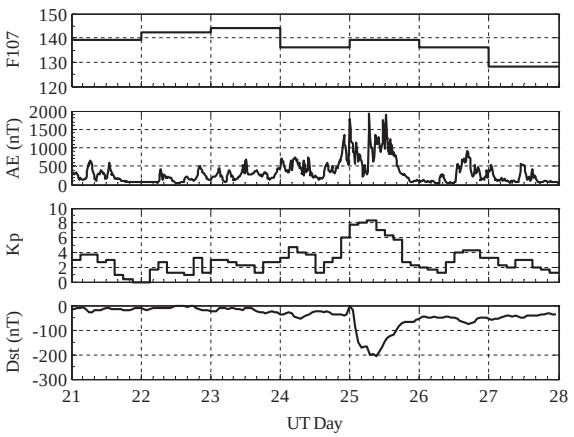

Fig. 1. The variations of F107, AE, K_p and D_{st} indices for September 21–27, 1998.

Evans, 1970). The observed N_mF_2 on September 25 shows a large negative phase compared to the reference day. After the SSC, a strong N_mF_2 decrease and an h_mF_2 increase were seen at nighttime. Then the daytime N_mF_2 was significantly reduced, and h_mF_2 was below 200 km (actually the F_1 peak height), known as "G condition". This feature can be seen frequently on mid-latitude ionograms, which is associated with the depleted N

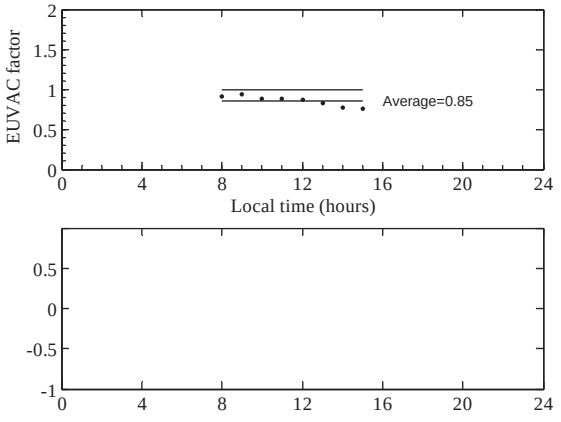
EUVAC factor
Average=0.85
Local time (hours)
2
1.5
1
0.5
0
-0.5
-1
0
4
8
12
16
20
24

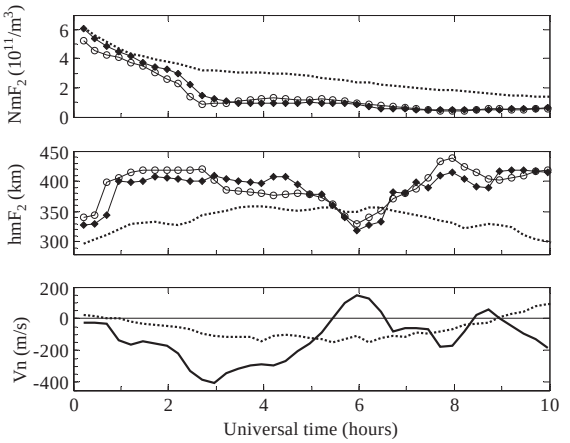

Fig. 8. The temporal variation of (a) N_mF_2 (the solid line with diamonds is the simulated values for September 25; For comparison, the observed values for September 25 (solid line with circles) and 22 (dotted line) are also presented), (b) h_mF_2, and the legends are the same as in the top panel, (c) the derived meridional neutral winds (positive poleward) for September 25 (solid line) and September 22 (dotted line) at h_mF_2.

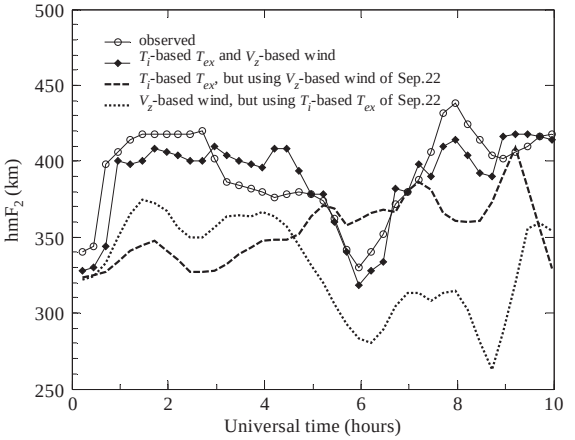

Fig. 9. Observed (solid lines with circles) and simulated h_mF_2 for the disturbed night of September 25, 1998. The solid line with diamonds shows the simulated h_mF_2 using T_i-based T_{ex} and V_z-based winds on September 25. The dashed line shows the simulated h_mF_2 using T_i-based T_{ex} on September 25, but using V_z-based winds of September 22 (quiet day) as the model input. The dotted line shows the simulated h_mF_2 using V_z-based winds of September 25, but using T_i-based T_{ex} of September 22 as the model input.

h_mF_2 and meridional winds on the nights of September 22 and 25. We can see that N_mF_2 decreases by a factor of 2.4 and a maximum h_mF_2 lifts by 114 km on September 25 from the level of September 22. After the onset of the magnetic storm, the h_mF_2 increased by 100 km between 0000 and 0300 UT, and then decreased continuously to a lowest value at 0600 UT, and rose again in the following hours. The rapid decrease in h_mF_2 around midnight had been studied previously by Nelson and Cogger (1971), namely the "midnight collapse" phenomenon. The modeled N_mF_2 and h_mF_2 (the solid lines with diamonds) show good agreement with the observed data. The meridional winds display stronger equatorward winds during 0000–0400 UT than those on September 22, and turn their directions from equatorward to poleward at $\sim$0515 and 0845 UT. This wave-like wind pattern is well reflected in the variation of h_mF_2. It may be caused by a travelling atmospheric disturbance (TAD), which behaves like large-scale gravity waves moving in the equatorward direction and carrying poleward winds (e.g., Schlesier and Buonsanto, 1999). As indicted by an increase in the AE index (Fig. 1), energy associated with the magnetospheric substorm is injected into the auroral upper atmosphere, probably launching a large-scale travelling atmospheric disturbance. This point deserves further investigation based on more data.

Further, numerical simulations are carried out to investigate the mechanism involved. Fig. 9 shows the simulated h_mF_2 for the disturbed night during 0000–1000 UT (1900–0500 LT) of September 25 for different cases required to examine the contributions of the dynamics effect and recombination processes to the h_mF_2 variation. The calculated h_mF_2 using T_i-based T_{ex} and V_z-based winds on September 25 is very close to the observation. When the V_z-based winds of September 22 are used instead of model input, h_mF_2 (dashed line) does not increase at the beginning while it is close to the observed h_mF_2 after 0600 UT. In another case, when the T_i-based T_{ex} of September 22 is used instead for the model input, h_mF_2 (dotted line) agrees with the observed data during 0000–0600 UT. In addition, we found that the electric fields (Fig. 3) have a slight effect on the simulated h_mF_2 (not shown). By comparing the three case results, it can be found that the process of the initial layer uplift and its consequent rise is mainly associated with the large equatorward winds. After 0600 UT, the increased recombination rate, which is caused by a large increase in T_{ex} (Fig. 5a) and by the increased molecular nitrogen and oxygen density, causes a great reduction of electron densities in the bottom-side F_2 layer and arouses the h_mF_2 rise again. The descent of the ionosphere ("midnight collapse") between these two intervals is due to the possible large-scale gravity wave (or TADs) (Fig. 8).

5. Summary and conclusions

A comparison of the model results of F-region electron density with the measurements at Millstone Hill during the September storm in 1998 has been carried out. The modeled densities based on the standard input parameters (climatological model values) are in agreement with the observed values, but there are some serious disagreements, requiring more exact information about the background atmosphere

than a general climatological description under quiet conditions. The model results show that the vibrationally excited N_2 and O_2 cannot explain the formation of negative storm in this case, although their effects would expect to become larger by using the derived T_{ex}. Thus, a data assimilation technique was used to deduce the exospheric temperature, winds, [O] and [N_2], and solar EUV flux from T_i and N_e profiles to understand the mechanisms of the storm effect.

The calculations showed large differences during storm time between the inferred neutral parameters from the Millstone Hill ISR data and the standard MRLMSISE-00 values. The maximum exospheric temperature T_{ex} derived from T_i profiles is higher than 1700 K, and differs from the NRLMSISE-00 model by 550 K on September 25. The calculated results show an averaged decrease in [O] at 300 km by a factor of 2.2 and an increase in [N_2] by $\sim$ 1:8 times on September 25 with respect to the corresponding parameters on September 22. The large [N_2]=[O] ratio can well explain the formation of G condition, and the significant negative phase at Millstone Hill during this storm.

A comparison of the simulated results with the observed data is carried out to investigate the relative importance of the dynamic effect and the chemical recombination process on the observed feature of a strong nighttime N_mF_2 decrease, accompanied by a large h_mF_2 increase after the sudden storm commencement (SSC). The inferred T_{ex} and the observed velocities are used in the calculations. We found that the uplift process in the F_2 layer from sunset to post-midnight is associated with the large equatorward winds, and the second rise in h_mF_2 after midnight results from the depleted electron density in the bottom-side of F_2 layer due to the increased recombination, while the "midnight collapse" of h_mF_2 is attributed to the large-scale traveling atmospheric disturbances associated with the substorm activity.

Acknowledgements

The MSIS and HWM models are provided by the World Data Center-A. Millstone Hill data were obtained through the Madrigal Database which is assembled and maintained by members of MIT Haystack Observatory Atmospheric Science Group. Special thanks are given to Prof. W.L. Oliver for providing the code of the heat balance calculation. This research was supported by the National Natural Science Foundation of China (40274054, 40134020) and the National Important Basic Research Project (G2000078407).

References

Anderson, D.N., Buonsanto, M.J., Codrescu, M., Decker, D., Fesen, C.G., FullerRowell, T.J., Reinisch, B.W., Richards, P.G., Roble, R.G., Schunk, R.W., Sojka, J.J., 1998. Intercomparison of physical models and observations of the ionosphere. Journal of Geophysical Research 103, 2179–2192.

Bauer, P., Waldteufel, P., Alcaydé, D., 1970. Diurnal variations of the atomic oxygen density and temperature determined from incoherent scatter measurements in the ionospheric F region. Journal of Geophysical Research 75, 4825–4832.

Buonsanto, M.J., Foster, J.C., 1993. Effects of magnetospheric electric fields and neutral winds on the low-middle latitude ionosphere during the March 20–21, storm. Journal of Geophysical Research 98, 19133–19140.

Buonsanto, M.J., 1999. Ionospheric storms-a review. Space Science Review 88, 563–601.

Chang, T., Torr, D.G., Richards, P.G., Solomon, S.C., 1993. Reevaluation of the $O^+(^2P)$ reaction rate coefficients from atmosphere explorer C observations. Journal of Geophysical Research 98, 15589–15597.

Danilov, A.D., Lastovička, J., 2001. Effects of geomagnetic storms on the ionosphere and atmosphere. International Journal of Geomagnetism and Aeronomy 2, 209–224.

Evans, J.V., 1970. Millstone-Hill Thomson scatter results for 1965. Planetary and Space Science 18, 1225–1252.

Fehsenfeld, F.C., 1977. The reaction of O_2^+ with atomic nitrogen and $NO^+ \cdot H_2O$ and NO_2^+ with atomic oxygen. Planetary and Space Science 25, 195–196.

Fox, J.L., Dalgarno, A., 1985. The vibrational distribution of N_2^+ in the terrestrial ionosphere. Journal of Geophysical Research 90, 7557–7567.

Hedin, A.E., 1987. MSIS-86 thermospheric model. Journal of Geophysical Research 92, 4649–4662.

Hedin, A.E., 1991. Extension of the MSIS thermospheric model into the middle and lower atmosphere. Journal of Geophysical Research 96, 1159–1172.

Hedin, A.E., Fleming, E.L., Manson, A.H., et al., 1996. Empirical wind model for the upper, middle and lower atmosphere. Journal of Atmospheric and Terrestrial Physics 58, 1421–1447.

Henry, R.J.W., Burke, P.G., Sinfailam, A.L., 1969. Scattering of the electron by C, N, O, N^+, O^+, and O^{++}. Physical Review 178, 218–224.

Hierl, P.M., Dotan, I., Seeley, J.V., Van Doren, J.M., Morris, R.A., Viggiano, A.A., 1997. Rate constants for the reactions of O^+ with N_2 and O_2 as a function of temperature (300–1800 K). Journal of Chemical Physics 106, 3540–3544.

Huba, J.D., Joyce, G., Fedder, J.A., 2000. Sami2 is another model of the ionosphere (SAMI2): a new low latitude ionospheric model. Journal of Geophysical Research 105, 23035–23053.

Johnsen, R., Biondi, M.A., 1980. Laboratory measurements of the $O^+(^2D) + N_2$ and $O^+(^2D) + O_2$ reaction rate coefficients and their ionospheric implications. Geophysical Research Letters 7, 401–403.

Kaufman, V., Sugar, J., 1986. Forbidden lines in $ns^2\ np^k$ ground configuration and nsnp excited configurations of Beryllium through Molybdenum atoms and ions. Journal of Physical and Chemical Reference Data 15, 321–426.

Lei, J., Liu, L., Wan, W., Zhang, S.-R., 2004. Model results for the ionospheric lower transition height over mid-latitude. Annales Geophysicae 22, in press.

Li, X., Huang, Y.-L., Flesch, G.D., Ng, C.Y., 1997. A state–selected study of the ion-molecule reactions $O^+(^4S, ^2D, ^2P) + N_2$. Journal of Chemical Physics 106, 1373–1381.

Lilensten, J., Blelly, P.L., 2002. The TEC and F2 parameters as tracers of the ionosphere and thermosphere. Journal of Atmospheric and Solar-Terrestrial Physics 64, 775–793.

Lindinger, W., Fehsenfeld, F.C., Schmeltekopf, A.L., Ferguson, E.E., 1974. Temperature dependence of some ionospheric

ion-neutral reactions from 300–900 K. Journal of Geophysical Research 79, 4753–4756.

Litvin, A., Oliver, W.L., Picone, J.M., Buonsanto, M.J., 2000. The upper atmosphere during June 5–11, 1991. Journal of Geophysical Research 105, 12789–12796.

Liu, L., Luan, X., Wan, W., Ning, B., Lei, J., 2003. A new approach to the derivation of dynamic information from ionosonde measurements. Annales Geophysicae 21, 2185–2191.

McFarland, M., Albritton, D.L., Fehsenfeld, F.C., Ferguson, E.E., Schmeltekopf, A.L., 1974. Energy dependence and branching ration of the $N_2^+ + O$ reaction. Journal of Geophysical Research 79, 2925–2926.

Mikhailov, A.V., Foster, J.C., 1997. Daytime thermosphere above Millstone Hill during severe geomagnetic storms. Journal of Geophysical Research 102, 17275–17282.

Mikhailov, A.V, Schlegel, K., 1997. Self-consistent modeling of the daytime electron density profile in the ionospheric F region. Annales Geophysicae 15, 314–326.

Mitra, A.P., 1968. A review of D-region process in non-polar latitudes. Journal of Atmospheric and Terrestrial Physics 30, 1065–1114.

Nelson, G.J., Cogger, L.L., 1971. Dynamical behavior of the nighttime ionosphere at Arecibo. Journal of Atmospheric and Terrestrial Physics 33, 1711–1726.

Oliver, W.L., 1979. Incoherent scatter radar studies of the daytime middle thermosphere. Annales de Géophysique 35, 121–139.

Pavlov, A.V., 1994. The role of vibrationally excited nitrogen in the formation of the mid-latitude negative ionospheric storms. Annales Geophysicae 12, 554–564.

Pavlov, A.V., Buonsanto, M.J., 1996. Using steady-state vibrational temperatures to model effects of N_2^* on calculations of electron densities. Journal of Geophysical Research 101, 26941–26945.

Pavlov, A.V., Buonsanto, M.J., 1997. Comparison of model electron densities and temperatures with Millstone Hill observations during undisturbed periods and the geomagnetic storms of 16–23 March and 6–12 April 1990. Annales Geophysicae 15, 327–344.

Pavlov, A.V., Buonsanto, M.J., Schlesier, A.C., Richards, P.G., 1999. Comparison of models and data at Millstone Hill during the 5–11 June 1991 storm. Journal of Atmospheric and Solar-Terrestrial Physics 61, 263–279.

Pavlov, A.V., Foster, J.C., 2001. Model/data comparison of F region ionospheric perturbation over Millstone Hill during the severe geomagnetic storm of July 15–16, 2000. Journal of Geophysical Research 106, 29051–29069.

Pesnell, W.D., Omidvar, K., Hoegy, W.R., 1993. Momentum transfer collision frequency of O^+–O. Geophysical Research Letters 20, 1343–1346.

Peterson, J.R., Padellec, A.Le., Danared, H., Dunn, G.H., Larsson, M., Larson, A., Peverall, P., Stromholm, C., Rosen, S., Ugglas, M., Van der Zande, W.J., 1998. Dissociative recombination and excitation of N_2^+: cross sections and product branching ration. Journal of Chemical Physics 108, 1978–1988.

Picone, J.M., Hedin, A.E., Drob, D.P., Aikin, A.C., 2002. NRLMSISE-00 empirical model of the atmosphere: statistical comparisons and scientific issues. Journal of Geophysical Research 107(A12), 1468, doi:10.1029/2002JA009430.

Prölss, G.W., 1993. On explaining the local time variation of ionospheric storm effects. Annales Geophysicae 11, 1–9.

Prölss, G.W., 1995. Ionospheric F-region storms. In: H. Volland (Ed.), Handbook of Atmospheric Electrodynamics. Vol. 2. CRC Press, Boca Raton, pp. 195–247.

Rees, M.H., 1989. Physics and Chemistry of the Upper Atmosphere. Cambridge University Press, Cambridge, pp. 125–126.

J;q2